Acoustic nonreciprocity in a lattice incorporating nonlinearity, asymmetry, and internal scale hierarchy: Experimental study

Jonathan Bunyan,[1] Keegan J. Moore,[1] Alireza Mojahed,[1] Matthew D. Fronk,[2] Michael Leamy,[2] Sameh Tawfick,[1,*] and Alexander F. Vakakis[1,†]

[1]*Mechanical Science and Engineering, University of Illinois, Urbana, Illinois, USA*

[2]*Mechanical Engineering, Georgia Institute of Technology, Atlanta, Georgia, USA*

(Received 24 January 2018; published 21 May 2018)

In linear time-invariant systems acoustic reciprocity holds by the Onsager-Casimir principle of microscopic reversibility, and it can be broken only by odd external biases, nonlinearities, or time-dependent properties. Recently it was shown that one-dimensional lattices composed of a finite number of identical nonlinear cells with internal scale hierarchy and asymmetry exhibit nonreciprocity both locally and globally. Considering a single cell composed of a large scale nonlinearly coupled to a small scale, *local dynamic nonreciprocity* corresponds to vibration energy transfer from the large to the small scale, but absence of energy transfer (and localization) from the small to the large scale. This has been recently proven both theoretically and experimentally. Then, considering the entire lattice, *global acoustic nonreciprocity* has been recently proven theoretically, corresponding to preferential energy transfer within the lattice under transient excitation applied at one of its boundaries, and absence of similar energy transfer (and localization) when the excitation is applied at its other boundary. This work provides experimental validation of the global acoustic nonreciprocity with a one-dimensional asymmetric lattice composed of three cells, with each cell incorporating nonlinearly coupled large and small scales. Due to the intentional asymmetry of the lattice, low impulsive excitations applied to one of its boundaries result in wave transmission through the lattice, whereas when the same excitations are applied to the other end, they lead in energy localization at the boundary and absence of wave transmission. This global nonreciprocity depends critically on energy (i.e., the intensity of the applied impulses), and reduced-order models recover the nonreciprocal acoustics and clarify the nonlinear mechanism generating nonreciprocity in this system.

DOI: 10.1103/PhysRevE.97.052211

I. INTRODUCTION

Reciprocity is a basic property in linear time-invariant (LTI) acoustic systems going back to the work of H. v. Helmholtz [1] and J. W. Strutt (Lord Rayleigh) [2]. It is a fundamental property of LTI acoustics and elastodynamics governed by self-adjoint operators and symmetric Green's functions [3]. Reciprocity is directly related to time-reversal symmetry through the Onsager-Casimir principle of microscopic reversibility [4–6], and breaking of reciprocity is only possible by breaking time reversal symmetry on the microlevel [7].

Recently, the study of the breaking of reciprocity in dynamical and acoustical systems has attracted considerable interest due to important potential applications, such as mechanical diodes, acoustic logic, preferential and irreversible propagation of sound, and targeted energy transfer in preferential directions within complex systems. Basic ways to break reciprocity (and time-reversal symmetry) in LTI systems is by applying odd-symmetric external biases [8–10], inducing time-variant properties [9,11,12], or incorporating nonlinearities [13–17]. Moreover, as shown in [18] breaking of reciprocity in nonlinear elastodynamics depends on the boundary conditions, the symmetries of the governing nonlinear operators, and the choice of the spatial points where the nonreciprocity criterion is tested. For a study of nonlinear nonreciprocal dynamics and acoustics of a finite, geometrically nonlinear, planar lattice behaving as a nonlinear "sonic vacuum" we refer to Zhang *et al.* [19].

In a recent study [20], a unit cell of two coupled oscillators was considered. It was composed of a grounded, weakly damped linear oscillator representing a large scale (LS) which was nonlinearly coupled to an ungrounded oscillator of smaller mass, representing a small scale (SS). Theoretical analysis and experimental testing of this nonlinear unit cell under impulsive excitation revealed that it exhibited nonreciprocity: When the LS was excited there occurred irreversible energy transfer to the SS, whereas when the SS was excited there occurred energy localization and absence of similar energy transfer to the LS. Since this nonreciprocal phenomenon occurred within a single unit cell it was referred to as local dynamic nonreciprocity. It was shown that the irreversibility and unidirectionality of the energy transfer from the LS to the SS was caused by the frequency-energy dependence of the strongly nonlinear (nearly nonlinearizable) stiffness coupling the two scales, yielding either early or delayed transient resonance captures in the transient dynamics. Generalization of nonreciprocity to unit cells composed of a LS coupled to multiple SSs was also discussed [20].

A natural extension of the previous study was carried out in another recent work [23] where the acoustics of a lattice composed of a finite number of the aforementioned unit

*tawfick@illinois.edu

†avakakis@illinois.edu

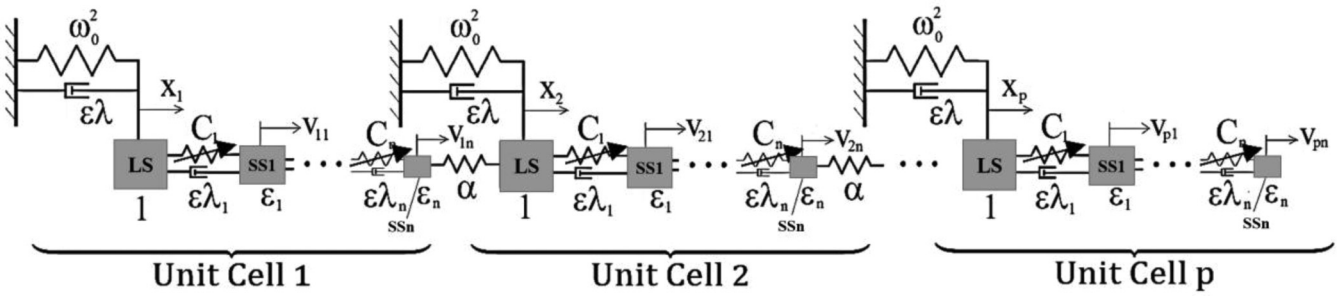

FIG. 1. The nonreciprocal lattice system composed of p linearly coupled unit cells; each unit cell is composed of a system of coupled oscillators in series, and incorporates strong stiffness nonlinearity, high asymmetry, and large-to-small scale hierarchy; LS denotes the large scale whereas SSk, $k = 1, \ldots, n$ denotes the small scales with decreasing mass as k increases.

cells was theoretically studied. Global acoustic nonreciprocity (By "acoustics" we refer to short-timescale, traveling waves or pulses [21] in media with local or nonlocal boundary effects [22], whereas by "dynamics" we denote long-timescale oscillations (standing waves) in finite media with nonlocal boundary effects.) was demonstrated in the lattice under both broadband and narrowband excitations: When the LS at one of the boundaries of the lattice was excited by a low-intensity excitation, energy was transmitted through the lattice in the form of traveling breathers, whereas when the same excitation was applied to the LS at the other boundary of the lattice it could not propagate through the lattice, but instead energy localization in the end cell occurred. As the intensity (energy) of the applied excitation increased, however, the acoustic nonreciprocity diminished, and, eventually, for relatively strong excitations wave transmission from both boundaries of the lattice occurred. The nonlinear mechanisms governing this global acoustic nonreciprocity were discussed in the same work [23].

The aim of the present study is to experimentally verify global acoustic nonreciprocity in a lattice of three identical unit cells, with each cell composed of two scales coupled by a strongly nonlinear stiffness. Asymmetry in the lattice is introduced by linearly coupling the LS of each unit cell to the SS of the unit cell to its right, and impulsive excitation is considered. A reduced-order model derived from system identification of the experimental lattice is used to reproduce and theoretically study the nonlinear mechanism that governs nonreciprocity in the lattice.

II. THEORETICAL OVERVIEW OF NONLINEAR NONRECIPROCITY

In this section we provide an overview of nonlinear nonreciprocity in a lattice incorporating nonlinearity, internal hierarchy, and asymmetry. As shown in Fig. 1 we consider a lattice system composed of p repeated, linearly coupled identical unit cells with internal nonlinear hierarchical structure. Introducing appropriate normalizations, each unit cell consists of a linear oscillator with unit mass grounded through the linear stiffness ω_0^2 in parallel to the weak viscous damping $\varepsilon\lambda$—representing the large scale – (LS) of the system—which is nonlinearly coupled to a series of n strongly nonlinear oscillators in series. These oscillators have increasingly smaller mass (or finer scale) and represent the small scales (SSs) of the unit cell (labeled as SS1–SSn). The kth small oscillator, SSk, has mass equal to $\varepsilon_k \ll 1$, with $\varepsilon_n \ll \varepsilon_{n-1} \ll \ldots \ll \varepsilon_k \ll \ldots \ll \varepsilon_1 \ll 1$ to enforce the internal hierarchy of small scales in the unit cell. In addition, the SSs are coupled to each other and to the LS by means of essentially nonlinear stiffness nonlinearities with pure (or nearly pure) cubic characteristics with stiffness constants $C_1, C_2, \ldots, C_n$, respectively, in parallel to the weak viscous dampers $\varepsilon\lambda_1, \ldots, \varepsilon\lambda_n$. As shown later a small linear component in the nonlinear stiffness characteristics would not significantly affect our results. Note that the weak linear viscous dampers of each unit cell are scaled by the small parameter $0 < \varepsilon \ll 1$. Asymmetry in the lattice is introduced through the coupling elements between cells; specifically, the smallest scale of each unit cell, SSn, is coupled to the LS of its adjacent LS of the unit cell on its right through the linear stiffness a. Exception is the last unit cell p, where the smallest scale lacks a coupling element.

Recently, nonreciprocity in the nonlinear lattice of Fig. 1 was theoretically established, both in a local and a global sense. Considering first each unit cell in isolation, it was shown both theoretically and experimentally [20] that local dynamic nonreciprocity occurs. Specifically, when the LS of the unit cell is forced by an impulsive excitation there is intense transfer of energy from the LS to the internal SSs. On the contrary, when the smallest scale (SSn) of the unit cell is excited by the same impulse the resulting nonlinear response is mainly localized to the smallest scale and the small scales that neighbor it, but no energy transfer to the LS is realized. It follows that nonreciprocal energy transfer from large to small scales within each unit cell occurs. Key to the local dynamic nonreciprocity is the strongly nonlinear coupling of the SSs, as the SSs have no preferential resonance frequencies due to their pure cubic stiffness; as such their oscillation frequencies are fully tunable with energy [20]. Assuming for simplicity that there is only a single SS, when the LS is impulsively excited a 1:1 transient resonance capture –(TRC) [24,25] occurs in the initial, high-energy regime of the transient dynamics as the SS tunes its instantaneous frequency to the (fixed linear) resonance frequency ω_0 of the LS, passively absorbing energy from it [26]; in this case this is the only characteristic frequency where resonance capture can occur in the system since the directly excited LS has the fixed preferential resonance frequency ω_0 (i.e., its frequency does not depend on the instantaneous energy of the LS). However, a completely different dynamics occurs where the small scale is impulsively excited, since in the initial,

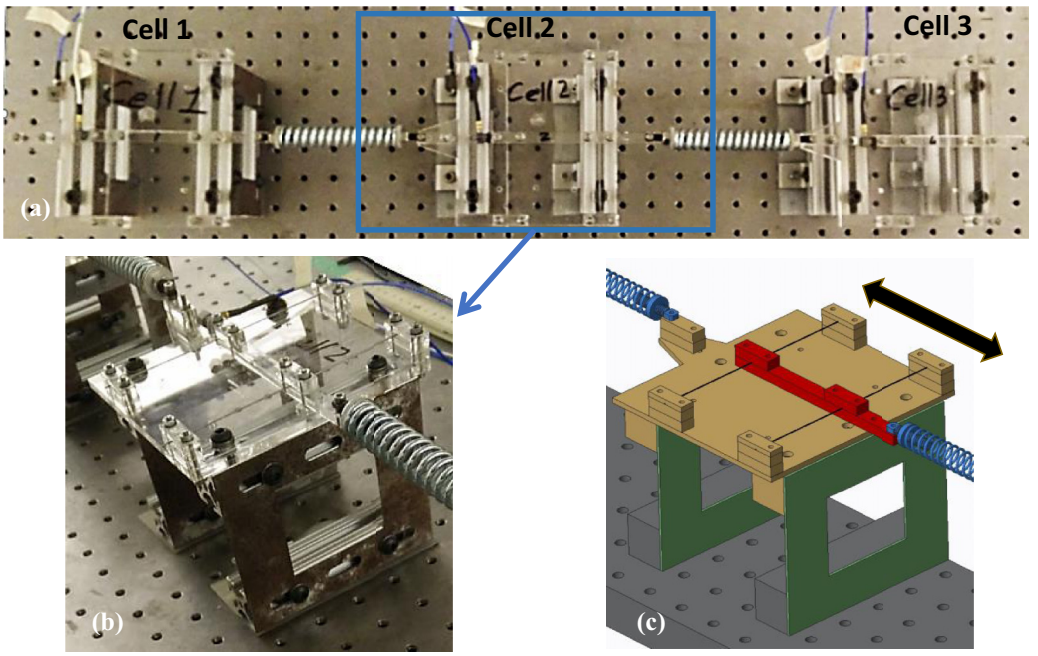

FIG. 2. Experimental three-cell lattice: (a) top view, (b) unit cell, and (c) schematic of the unit cell—yellow parts constitute the large scale (LS), red parts the small scale (SS), blue elements the linear coupling springs between cells, green parts the linear grounding stiffness of the LS, and the two transverse wires suspend the (lightweight) SS and generate the strong nonlinear stiffness coupling the LS to the SS. The wires are marked by blue arrows.

high-energy regime of the transient dynamics the instantaneous oscillation frequency of the SS is relatively high ($\gg \omega_0$) since its stiffening response is tunable with energy and its frequency increases with increasing energy; in this case there is no characteristic frequency for resonance capture in the initial high-energy regime, and resonance capture at the characteristic frequency ω_0 can only occur after sufficient reduction of the frequency of the SS occurs due to viscous damping dissipation. In that case, no 1:1 TRC can occur in the initial highly energetic regime of the response, but rather, only delayed 1:1 TRC with the LS can be realized at a reduced-energy regime after the instantaneous frequency of the SS decreases due to energy viscous dissipation and becomes comparable to the linear resonance frequency ω_0. This restricts the amount of energy that can be transferred from the SS to the LS at the regime of the delayed 1:1 TRC and yields energy localization in the SSs.

Considering then the lattice of Fig. 1 in its entirety it was computationally proved [23] that global acoustic nonreciprocity occurs. Hence, it was shown that strong nonreciprocity in the scale of each unit cell and in the scale of all unit cells in unison occurs. Note that the smallest scale (innermost oscillator) of each hierarchical unit cell is coupled to the large scale (outer oscillator) of the next unit cell on its right via a linear stiffness in such a manner as to break left-to-right (L-R) and right-to-left (R-L) symmetry. This asymmetry, combined with the strong nonlinearity in each cell, leads to globally nonreciprocal acoustics:

(1) L-R: Propagating waves transfer energy from the large to the smaller scales (LS to SSs) via TRCs. The smallest internal scale then transfers energy to the LS of the next (right) cell via linear coupling; energy transfer and propagation continue.

(2) R-L: Propagating waves arrive at the smallest scale of a cell via linear coupling from the LS of the cell on its right, but due to restricted SS to LS energy transfer, the wave is arrested.

Note that the internal nonlinear scale hierarchy (asymmetry) of the cells also breaks time-reversal symmetry. In forward time leftward propagating disturbances transfer energy from the LSs to the inner SSs within a cell, and then across cells (to LSs) via the linear coupling; this propagation is consistent with the preferred energy transfer direction. Upon time reversal, this propagation would violate the preferred small-to-large scale energy transfer direction.

The aim of this work is to experimentally validate acoustic nonreciprocity in a three-cell nonlinear lattice of the general configuration of Fig. 1, incorporating two-scale internal hierarchy (a LS and a SS in each unit cell) and linear coupling between cells. Then, the experimental results will be matched with a reduced-order model from system identification.

III. EXPERIMENTAL FIXTURE AND REDUCED-ORDER MODELING THROUGH SYSTEM IDENTIFICATION

The experimental lattice composed of three unit cells (labeled as cells 1–3) is depicted in Fig. 2, together with a schematic representation of a unit cell indicating how strong nonlinearity, internal scale hierarchy and linear coupling are realized. Each unit cell is composed of a LS coupled to a SS, both oscillating in the direction indicated by the double-sided arrow in Fig. 2(c). Adjacent cells are coupled by linear springs. All LSs and SSs were fabricated with acrylic and were laser cut to shape. Each LS was grounded to an optical table using 80/20 T-slotted aluminum extrusions, aluminum L-brackets, steel flexures, and bolts. The steel flexures served as the linear grounding stiffnesses and were bolted to the 80/20 members.

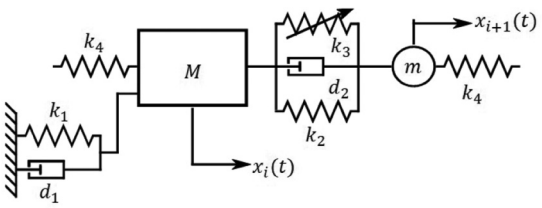

FIG. 3. The reduced-order model (ROM) of the unit cell of the experimental fixture of Fig. 2.

To achieve strong nonlinearity, the (lightweight) SS in each unit cell was suspended from the corresponding LS using two parallel, initially untensioned, steel wires of 0.035 in. thickness, with fixed ends; these were realized by clamping the two wires to the LS using thin acrylic strips to obtain the required cubic nonlinearity.

In theory, provided that the wires are initially untensioned and obey the classic wave equation, under transverse deformation at their center they act as strongly nonlinear, nearly cubic springs; that is, their force-displacement law is approximately cubic with no linear component [27,28]. However, in practice, due to their thickness, the wires always possess a small bending stiffness, so they behave more like thin Euler-Bernoulli beams instead of strings. This gives rise to a small linear stiffness in addition to the strongly nonlinear stiffness, but this does not affect the nonreciprocity. It follows that a small linear term in the spring that couples the LS and SS is unavoidable in practice, but this can be made small by reducing as much as possible the thickness-to-length ratio of the clamped wires.

Prior to performing the experimental tests for acoustic nonreciprocity, characterization of the experimental three-cell lattice was conducted, and a six degree-of-freedom (DOF) reduced-order model (ROM) was constructed. To this end, the two-DOF ROM of each of the three experimental unit cells is presented in Fig. 3, where M and m are the masses of the LS and the SS, k_1 and d_1 are the linear stiffness and linear viscous damper of the grounding connection of the LS, k_3 and d_2 are the nonlinear (cubic) stiffness and linear viscous damper connection between the LS and the SS, and k_4 is the linear stiffness coupling the SS of the ith unit cell to the LS of the $(i+1)$-th unit cell of the lattice. In addition, a small linear part (due to a small wire pretension) has been identified in the nonlinear connection between the LS and SS of each unit cell, and this is denoted by the linear stiffness k_2. Accordingly, the ROM of the experimental lattice is governed by the following set of ordinary differential equations with zero initial conditions:

$$\begin{aligned} &M\ddot{x}_i + d_1\dot{x}_i + d_2(\dot{x}_i - \dot{x}_{i+1}) + k_1x_i + k_2(x_i - x_{i+1}) \\ &+ k_3(x_i - x_{i+1})^3 + k_4(x_i - x_{i-1})(1-\delta_{i1}) = F_i(t) \\ &m\ddot{x}_{i+1} - d_2(\dot{x}_i - \dot{x}_{i+1}) - k_2(x_i - x_{i+1}) \\ &\quad - k_3(x_i - x_{i+1})^3 + k_4(x_{i+1} - x_{i+2})(1-\delta_{i5}) = 0 \\ &x_i(0) = \dot{x}_i(0) = x_{i+1}(0) = \dot{x}_{i+1}(0) = 0,\ i = 1,3,5, \end{aligned} \quad (1)$$

where δ_{ij} is the Kronecker delta symbol, indicating that the LS of unit cell 1 and the SS of unit cell 3 are not coupled to a SS and LS, respectively. As mentioned previously the coupling configuration between the LSs and SSs of the unit cells is the source of asymmetry in the lattice which is one of basic prerequisites for the realization of acoustic nonreciprocity [23]. Moreover, for generality we account for excitation of each of the LSs of the unit cells, as indicated by the forcing functions $F_i(t)$, $i = 1,3,5$.

The characterization of the experimental lattice was performed by nonlinear system identification [29–33]. The aim of the identification exercise was to estimate the parameters of the two-DOF ROM of each of the three unit cells (cf. Fig. 3) so that the overall six-DOF ROM of the experimental lattice reproduces (predicts) as close as possible the experimental measurements under varying impulsive forcing conditions. Then, after its validation the mathematical ROM could be used (i) to confirm that the experimental results indeed reproduced the theoretically predicted nonlinear acoustics, and (ii) to perform predictive design, i.e., for parametric studies and optimization of the nonlinear acoustic nonreciprocity. To achieve this we optimized the system parameters of the model of Fig. 3 of each unit cell so that the simulation transient responses matched as closely as possible the experimental measurements.

First, the system parameters of each unit cell were identified by decoupling it from the lattice [i.e., by setting $k_4 = 0$ in the ROM (1)] and characterizing it separately. The masses of the LS and SS of each unit cell of the experimental lattice were directly measured. Then, an impulsive load of small magnitude (to excite mainly the linearized dynamics of the unit cell) was applied to the LS of each decoupled unit cell by means of a modal hammer, and the corresponding transient accelerations of the LS and the SS were measured by means of accelerometers. In the next step, the accelerations were numerically integrated and the resulting velocities were high-pass filtered using a third-order Butterworth filter with a cutoff frequency of 20 Hz. By performing a fast Fourier transform (FFT) to the velocity time series two linearized natural frequencies (peaks) were identified in the FFT plot corresponding to two linearized modes of the cell. One of these frequencies was due to the linear grounding spring (k_1) of the LS. The other was caused by a linear component in the coupling spring between the LS and the SS (k_2). System identification analysis of the FFT results yielded good initial estimates of the linear components of the grounding and coupling stiffnesses of each unit cell.

The final identification of the system parameters of the ROM of each decoupled unit cell was performed by optimally matching the simulated ROM and the experimentally measured transient responses. To accomplish this, the response of the ROM of each decoupled unit cell subject to the actual experimental impulsive force (which was interpolated in the time domain) was simulated using MATLAB'S ODE45, and the optimization was carried out using MATLAB'S PATTERNSEARCH algorithm with the objective to minimize the following ratio,

$$P = \frac{\sum_{t_k}\left[u^{\mathrm{expt}}(t_k) - u^{\mathrm{sim}}(t_k)\right]^2}{\sum_{t_k}\left[u^{\mathrm{expt}}(t_k) - \bar{u}^{\mathrm{sim}}(t_k)\right]^2} + \frac{\sum_{t_k}\left[v^{\mathrm{expt}}(t_k) - v^{\mathrm{sim}}(t_k)\right]^2}{\sum_{t_k}\left[v^{\mathrm{expt}}(t_k) - \bar{v}^{\mathrm{sim}}(t_k)\right]^2}, \quad (2)$$

where the overbar denotes temporal mean; t_k the discrete time instants where the responses are computed; the superscripts

"expt" and "sim" refer to experimental and simulated time series, respectively; and u, v refer to the transient velocity responses of the LS and the SS of the decoupled unit cell, respectively. We note that the minimization of the ratio P is equivalent to the maximization of the R-squared fit between the simulated and experimentally measured velocity time series simultaneously for the both the LS and SS of the unit cell.

As a second step, the linear springs coupling adjacent unit cells were identified by removing the SSs and the nonlinear stiffness elements from the cells of the lattice, and coupling pairs of the resulting linear LSs through the coupling springs. Applying the restoring force method [29,30] to the resulting linear fixture of two coupled LSs yields accurate identification of the linear coupling springs, and, in addition, verification of the absence of any dissipative effects. This completed the characterization of the experimental lattice.

The identified system parameters of the unit cells of the experimental lattice are listed in Table I. We note that the unit cells are not identical, but rather small variations of the system parameters are estimated; this is inevitable due to manufacturing, material and geometrical imperfections, as well as uncertainties and unmodeled effects in the system identification procedure. Yet, as shown in a later section these small imperfections do not affect in any significant way the realization of acoustic nonreciprocity in the experimental lattice.

As an example of the efficacy of the nonlinear system identification, in Fig. 4 we depict the comparison between the experimentally measured velocity time series and the corresponding predicted simulated results of the ROM of the uncoupled unit cell 2 for impulsive excitation of the LS of the unit cell with maximum magnitude equaling 17.3 N. These experimental responses were used for identifying the ROM of the uncoupled unit cell 2. The responses of the LS and the SS of the unit cell are considered separately in Figs. 4(a) and 4(b), respectively, and comparisons of the velocity time series, the corresponding modulus of their continuous wavelet transform spectra, and the corresponding FFTs are provided in each case. We note that the identified ROM accurately reproduces the experimental measurements, validating the system identification procedure. As a further test of the accuracy and robustness of the identified ROM, in Fig. 5 we depict the analogous comparisons for the case of a higher magnitude impulse applied to the LS where it is anticipated that the nonlinear effects are more profound. For the comparisons shown in Fig. 5 the ROMs identified from the experimental time series of Fig. 4 were used. Yet, the responses of the ROM accurately capture the nonlinear measured responses even for this higher-energy (and stronger nonlinear) case, which validates the identified ROM.

TABLE I. Identified system parameters of the ROM of the experimental lattice.

Parameter	Unit cell 1	Unit cell 2	Unit cell 3
M (kg)	0.4349	0.4385	0.4325
m (kg)	0.0204	0.0206	0.0202
k_1 (N/m)	30166	35014	31306
k_2 (N/m)	1598.2	1571.8	1756.6
k_3 (N/m^3)	5×10^8	1×10^8	3×10^8
d_1 (Ns/m)	4.5	4.5	4.25
d_2 (Ns/m)	0.18	0.18	0.15
k_4 (N/m)	3753.75	3753.75	3753.75

IV. EXPERIMENTAL MEASUREMENT OF NONLINEAR ACOUSTIC NONRECIPROCITY IN THE LATTICE

In the experimental study, the three-cell lattice was forced by impulsive excitations applied sequentially to the LSs of the unit cells at its left and right boundaries. Specifically, impulsive excitations of varying intensity were applied first to the LS of unit cell 1 [cf. Fig. 2(a)], and then to the LS of unit cell 3 by means of a modal impact hammer. The acceleration time series of the LSs of all three unit cells of the lattice were measured by attached accelerometers, and from these measurements the velocity and displacement time series could be obtained using numerical integration and high-pass filtering. In [23], it was theoretically predicted that for sufficiently low-intensity impulsive loads strong acoustic nonreciprocity occurs, in the sense that waves generated due to excitation of (the left) unit cell 1 propagated through the lattice (i.e., there occurred L-R wave propagation); on the contrary, when (the right) unit cell 3 was forced by similar low-intensity impulsive loads there occurred localization of the response in that cell and absence of R-L wave propagation. However, for sufficiently high-intensity impulsive excitations, although the acoustic nonreciprocity persisted, localization was eliminated and both L-R and R-L wave propagation in the lattice occurred.

The theoretically predicted global acoustic nonreciprocity phenomena were fully confirmed experimentally with the three-cell lattice of Fig. 2. Our study involved numerous experimental tests corresponding to impulsive excitations of varying intensity, but in this work, we present only three representative experimental cases corresponding to impulsive excitations of low (cf. Fig. 6), intermediate (cf. Fig. 7), and high intensity (cf. Fig. 8). In each case we forced the lattice by impulsive excitations applied separately at cells 1 and 3; we note that, whereas exact replication of the left and right impulsive loads was not possible experimentally, the applied excitations ended up being nearly similar (in each case we report the maximum magnitudes of the impulsive excitations applied to cells 1 and 3). For each case of impulse excitation, we depict plots showing the spatiotemporal variation of the normalized (with respect to the total input impulsive energy) instantaneous energies of the three cells of the lattice; these plots were constructed by computing the potential and kinetic energy of each unit cell, depicting them in contour plots in space and time, and interpolating the results to get continuous graphs. In addition, we depict the temporal variations of the non-normalized total energy of the lattice following the application of the impulsive load, together with the temporal variations of the non-normalized energies of each of the three cells. These plots show the overall energy decay in the experimental lattice following the impulsive excitation, as well as interesting energy exchanges between unit cells. Finally, as a direct measure of global acoustic nonreciprocity in the lattice, we compare the response of the LS of cell 1 when the impulsive excitation is applied to the LS of cell 3, to the response of the LS of cell 3 when a similar impulse excitation is applied to

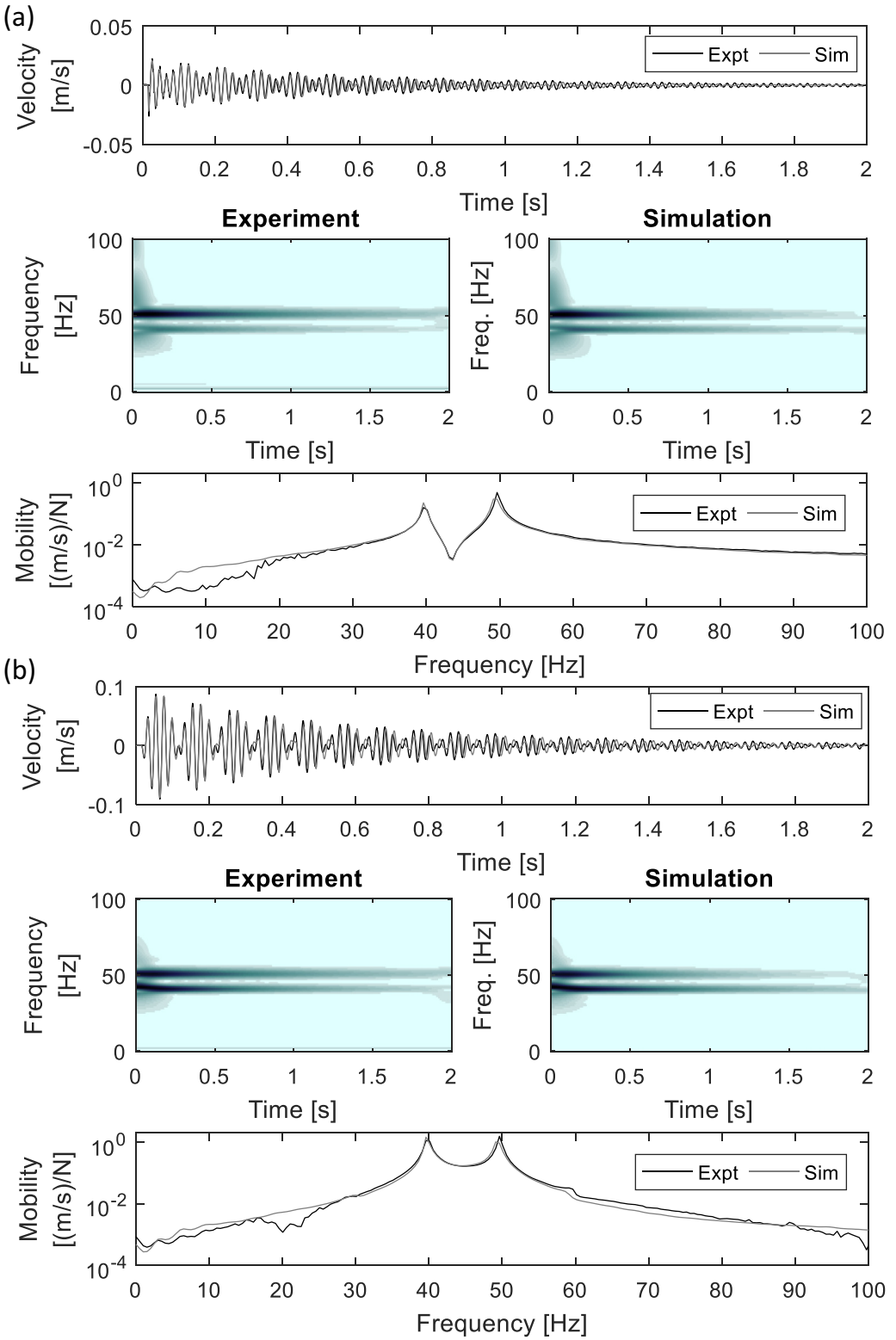

FIG. 4. Comparison of experimental and identified ROM responses for the uncoupled unit cell 2, impulse of maximum magnitude 17.3 N applied to the LS: (a) LS, and (b) SS responses; this experimental test was used to identify the ROM of the unit cell.

the LS of cell 1. These experimental plots depict clearly the propagating or localized nature of the lattice response when excited at the LSs on its left or right boundary cells.

Considering first the case of low-intensity impulsive loads depicted in Fig. 6 we clearly deduce the realization of nonreciprocal acoustics in the lattice. Specifically, considering the

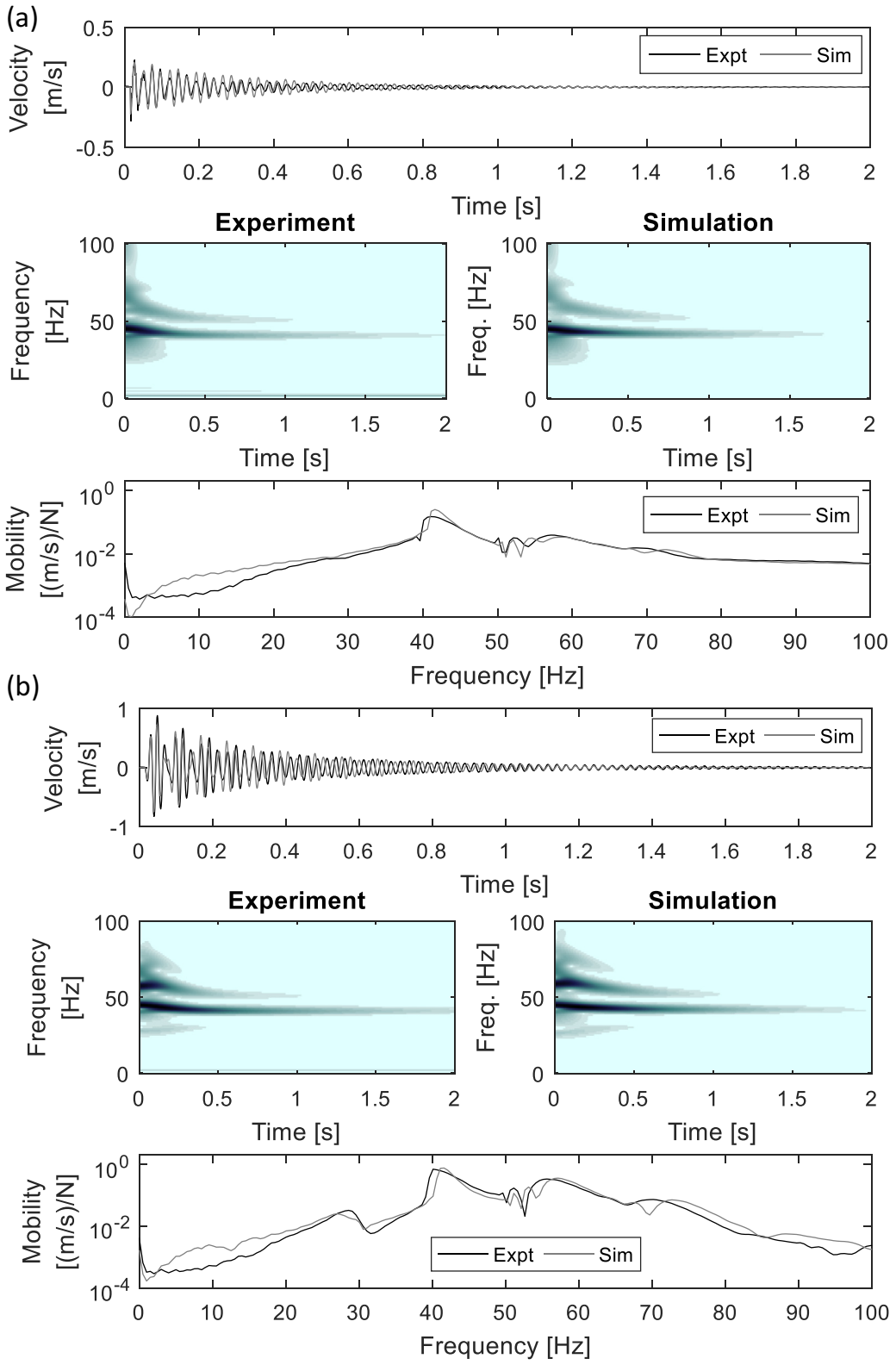

FIG. 5. Comparison of experimental and identified ROM responses for the uncoupled unit cell 2, of maximum magnitude 281.6 N s applied to the LS: (a) LS, and (b) SS responses; the ROM of the unit cell was identified based on the experimental test depicted in Fig. 4.

spatiotemporal normalized energy variations in Figs. 6(a) and 6(b) we note wave transmission and response localization when unit cells 1 and 3 are excited, respectively. The global acoustic nonreciprocity in this case is further confirmed by the plots of energy variations, where for excitation applied to the left cell 1 energy exchanges (beats) occur between all three unit cells, whereas for similar excitation applied to the right end cell 3 we deduce energy localization in that cell. Moreover, judging from

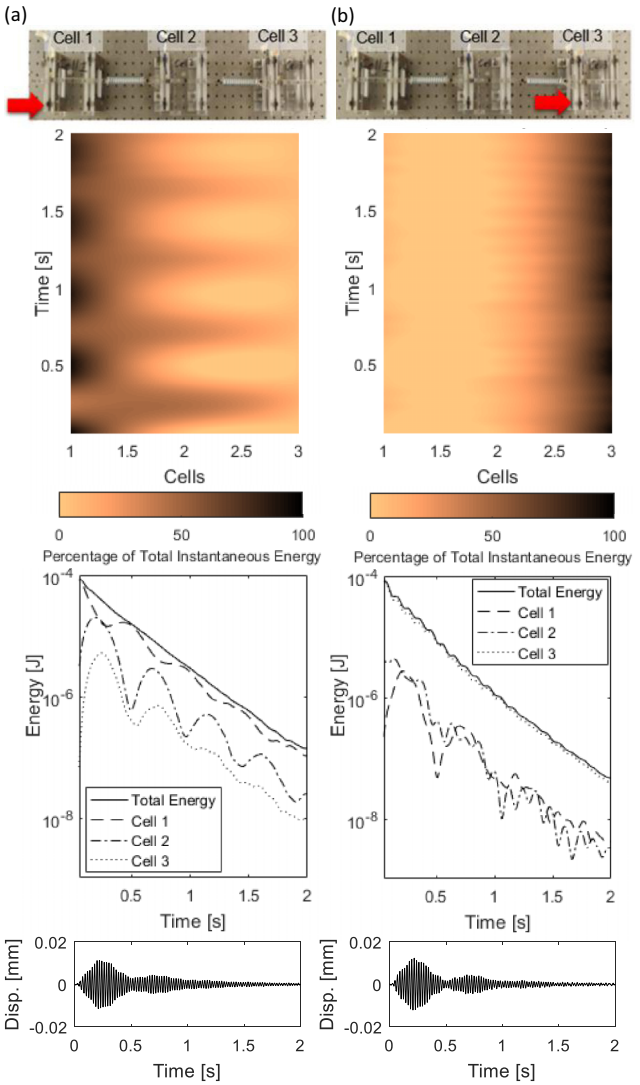

FIG. 6. Small impulsive intensity: (a) impulsive magnitude 15.28 N applied to cell 1, (b) impulsive magnitude 18.01 N applied to cell 3: spatiotemporal variation of normalized energy (with respect to input energy) for each cell (top), temporal variations of the lattice energy and the non-normalized energy of each cell (middle), and LS response of cell 3 (cell 1) when the LS of cell 1 (cell 3) is excited (bottom).

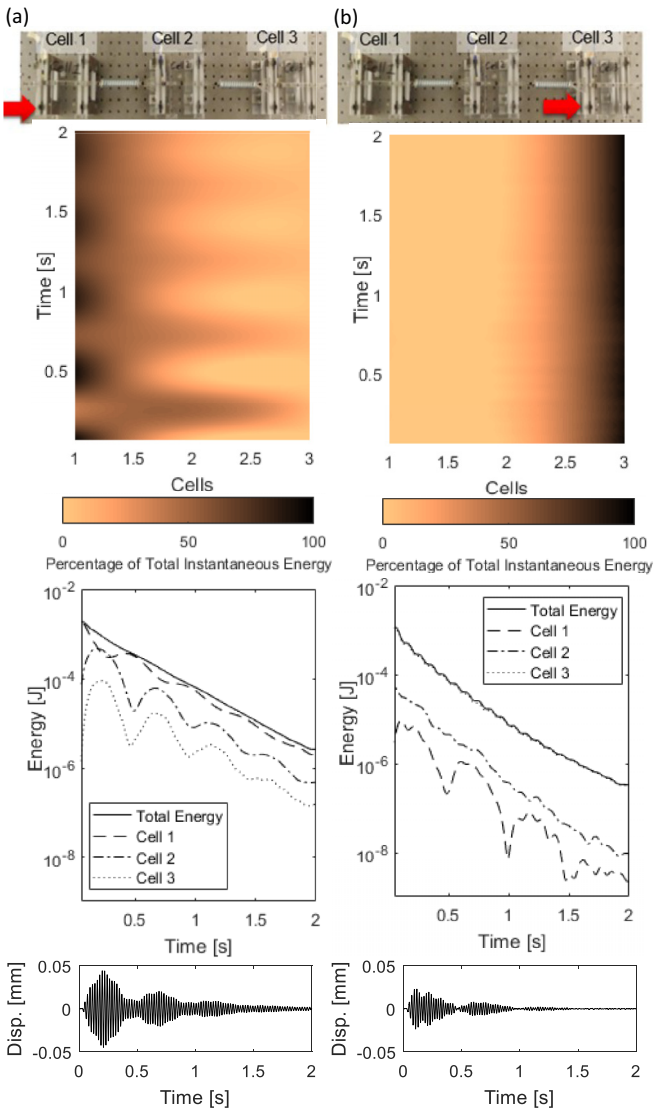

FIG. 7. Intermediate impulsive intensity: (a) impulsive magnitude 102.04 N applied to cell 1, (b) impulsive magnitude 96.19 N applied to cell 3: spatiotemporal variation of normalized energy (with respect to input energy) for each cell (top), temporal variations of the lattice energy and the non-normalized energy of each cell (middle), and LS response of cell 3 (cell 1) when the LS of cell 1 (cell 3) is excited (bottom).

the decay of the overall energy of the lattice in these two plots, it is interesting to note that for excitation applied to cell 3 the overall energy decay in the lattice is faster, which indicates that response localization in cell 3 results in more efficient overall energy dissipation in the lattice. Finally, we note that for this low-intensity excitation the response of the LS of cell 1 when the impulse is applied to cell 3 is similar to the response of the LS of cell 3 when a similar impulse is applied to cell 1, with their difference being of $\mathcal{O}(10^{-6}$ m).

Considering the case of intermediate-intensity impulsive loads (∼100 N) depicted in Fig. 7 we note similar nonlinear acoustic nonreciprocity in the lattice, with L-R wave transmission when unit cell 1 is excited, and response localization when the impulsive excitation is applied to unit cell 3. In this case the global acoustic nonreciprocity is more profound compared to the previous low-intensity load case, as indicated by the relatively large difference in the time series of the cell responses, which now is on the order of $\mathcal{O}(10^{-5}$ m). In addition, for impulsive excitation applied to cell 1 the energy exchanges between cells are more pronounced, as can be deduced from the temporal energy variations in Figs. 7(a) and 7(b). From the same plots we note much more efficient overall energy dissipation when cell 3 is excited (case of localization), compared to when cell 1 is excited (case of L-R wave propagation).

Finally, the case of high-intensity applied loads (∼800 N) is depicted in Fig. 8, where qualitatively different nonlinear acoustics are noted in the lattice. As the time series comparisons of Fig. 8 indicate there is strong acoustic nonreciprocity

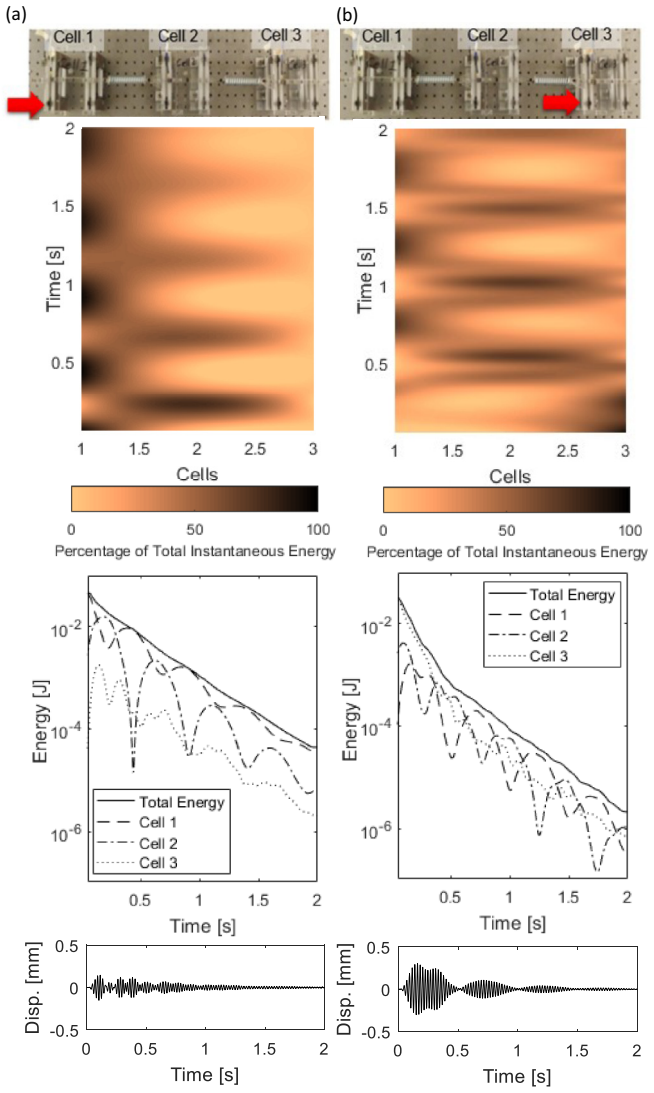

FIG. 8. Intermediate impulsive intensity: (a) impulsive magnitude 856.99 N applied to cell 1, (b) impulsive magnitude 835.72 N applied to cell 3: spatiotemporal variation of normalized energy (with respect to input energy) for each cell (top), temporal variations of the lattice energy and the non-normalized energy of each cell (middle), and LS response of cell 3 (cell 1) when the LS of cell 1 (cell 3) is excited (bottom).

in this case, but both L-R and R-L wave propagation is realized and there is absence of response localization when the unit cell 3 is excited by the impulsive load (as in the previous two cases); this result is in full agreement with the theoretical predictions of Fronk *et al.* [23]. Another qualitative difference of the nonlinear acoustics in this case compared to the low- and intermediate-intensity impulse cases, is that the response of cell 1 when cell 3 is impulsively excited is now much higher than the response of cell 3 when cell 1 is excited. This result, which correlates with the spatiotemporal normalized energy plots of Figs. 8(a) and 8(b), reveals that for high-intensity impulse excitation R-L wave propagation is much stronger than L-R wave propagation; this result contrasts with the results of Figs. 6 and 7, where only L-R wave propagation occurred. Finally, similar to the previous cases there is much stronger overall energy dissipation in the lattice when cell 3 is impulsively excited, compared to when cell 1 is excited. This can be clearly deduced by the overall energy decay plots shown in Figs. 8(a) and 8(b). From these plots we note that for high-intensity impulsive excitation there occur energy exchanges between cells for both left- and right-applied loads, confirming L-R and R-L wave propagation in this case.

At this point, we comment on the possible origin of nonreciprocity in the lattice. The asymmetric localization in the system response seems to be caused by the specific arrangement and coupling of the cells. In the studied configuration the "free" SS of the right-end cell 3 is activated briefly after the application of the impulse to the LS of cell 3, and, in essence, behaves as a nonlinear energy sink (NES) in resonance, absorbing and dissipating a considerable amount of the input energy; as a result, motion localization occurs in cell 3. On the contrary, when the LS of the left-end cell 1 is excited by an impulse, the corresponding SS of that cell is not "free" to act as a NES since it is linearly coupled to the LS of the neighboring cell 2. As a result, there is absence of localization when the left cell 1 is excited by the impulse, so wave propagation through the lattice occurs. Comparing the L-R and R-L excitation cases we conclude that the "free" SS mass in cell 3 should play a significant role in the energy localization, acting as a NES. Moreover, it has been shown that the effectiveness of a NES to dissipate energy strongly depends on the input energy; at low input energy levels the NES is not activated to its full capacity, but at intermediate input energy levels the energy dissipated by the NES grows and reaches a peak value [26]. As the input energy further increases the effectiveness of the NES to absorb and dissipate input energy diminishes [26]. It is conjectured at this time that the same mechanism holds for the hierarchical lattice: In the R-L configuration at low to intermediate energy levels the NES dissipates a significant portion of the input energy which leads to localization of energy at the right side of the system; however, as the input energy increases and the maximum dissipative capacity of the NES is exceeded, a smaller fraction of the input energy is dissipated locally by the NES in cell 3, and the remaining energy is released to propagate through the lattice.

Summarizing, the experimental tests confirm fully the theoretical predictions of Fronk *et al.* [23] and prove experimentally the realization of strong nonlinear acoustic nonreciprocity in the three-cell lattice of Fig. 2. For low- and intermediate-intensity applied impulsive loads there occurs only L-R wave propagation in the lattice, and strong response localization when the right cell was excited. Increasing the impulse intensity eliminates the localization phenomenon and both L-R and R-L wave propagation occurs in the lattice. In all cases, however, strong global acoustic nonreciprocity occurs in this nonlinear, asymmetric, hierarchical lattice. This nonreciprocity affects drastically the dissipative capacity of the lattice, with impulsive excitations applied to cell 3 yielding much stronger dissipation of energy. Additional experimental tests with different magnitudes of impulsive excitations confirmed these findings.

We attempt to describe the nonreciprocity more quantitatively. We note at this point that, while the spatiotemporal energy plots are a good way to assess energy distribution,

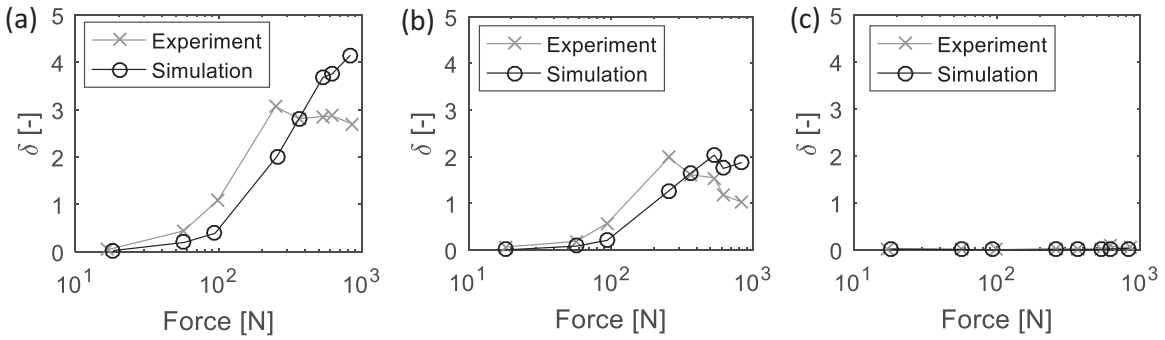

FIG. 9. Nonreciprocity measure δ based on the responses of the LSs of the three cells of the lattice: (a) LSs in cells 1 and 3, (b) LSs in cells 2 and 3, and (c) LSs in cells 1 and 2; both experimental data (grey) and simulated data (black) are considered at various impulse intensities.

and distinguish between the different types of nonreciprocal responses (i.e., localization versus wave propagation when the system is forced from the left or the right), the normalization at each time step in the plots with respect to the total instantaneous energy in the system does not help to assess quantitatively the nonreciprocity in the system. As a result, the spatiotemporal energy plots of Fig. 6–8 cannot be used directly to assess quantitatively the degree of nonreciprocity in the system, and should only be used to distinguish between the regimes of energy localization or transmission. Instead, to measure quantitatively the degree of acoustic nonreciprocity in the system and its evolution as energy increases, another measure is considered as follows. Based on the adopted forcing protocol of this study, i.e., sequential excitation of the system at two different points of the lattice using the same force, say, i and j, a measure of the normalized difference of the corresponding responses at these points is computed, and a "global" measure of nonreciprocity, $\delta[x_i,x_j]$, in the lattice is calculated following the scheme used by Blanchard *et al.* [18] and Herrera *et al.* [34],

$$\delta[x_i,x_j] = \frac{\frac{1}{T}\int_0^T (x_i - x_j)^2 dt}{\sqrt{\frac{1}{T}\int_0^T (x_i)^2 dt}\sqrt{\frac{1}{T}\int_0^T (x_j)^2 dt}}, \qquad (3)$$

where T is the time window of the data record based on which the measure is computed, and x_i and x_j are the corresponding responses at the reciprocal points i and j. Based on its definition, $\delta[x_i,x_j]$ provides a direct quantitative measure to assess nonreciprocity in the lattice. In the following results we considered the LSs of each of the three cells as the measurement points, and assembled them in pairs to compute the nonreciprocity measure (3) based on the recorded responses. In Fig. 9 the resulting measure δ for various impulse intensities is depicted. Note that in a fully reciprocal system the measure should vanish, i.e., $\delta = 0$, for any combination of reciprocal points i and j, and at any excitation level. The results for the nonlinear lattice of our study are rather interesting.

First, nonreciprocity in the lattice only manifests when the end cell 3 is considered as one of the measurement points indicating the important role that the "free" SS of the right-end cell 3 plays in nonreciprocity.

Second, nonreciprocity appears to increase with increasing force intensity, in spite of the fact that there are different response regimes in the lattice with increasing energy, i.e., motion localization at cell 3 versus wave propagation for increasing energy. Indeed, at the lower impulse intensities the apparent nonreciprocity observed at all measurement points is small even though the distribution of energy throughout the system is fundamentally different (cf. Fig. 6). However, at larger impulse intensities strong nonreciprocity is still maintained even though the localization phenomenon is lost (cf. Fig. 8), indicating that the nonreciprocity and localization phenomenon are distinct phenomena. Interestingly, a global

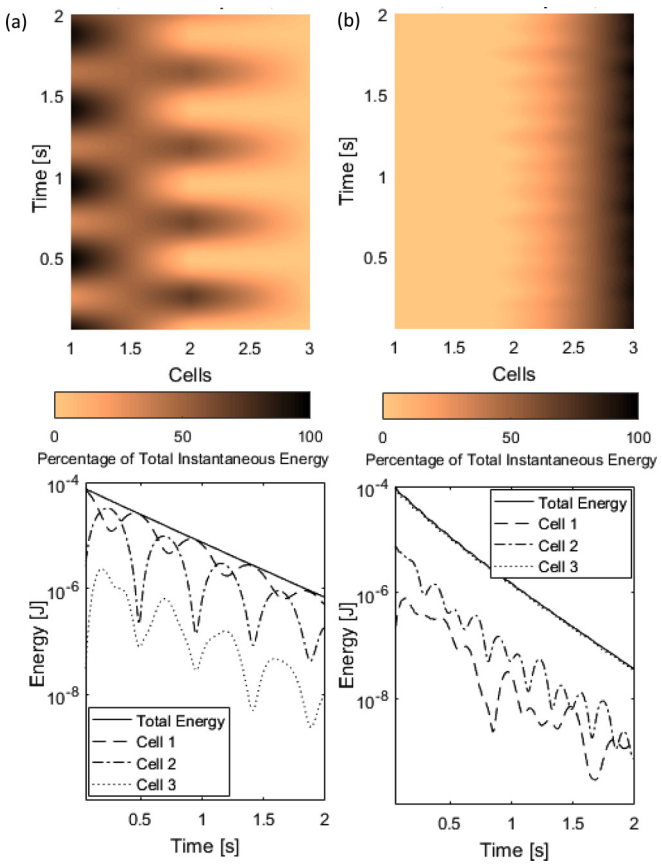

FIG. 10. Numerical simulation results of the ROM for small impulsive intensity, impulsive magnitude 15.28 N applied to cell 1, and impulsive magnitude 18.01 N applied to cell 3: (a) spatiotemporal variation of normalized energy (with respect to input energy) for each cell, and (b) and temporal variations of the lattice energy and the non-normalized energy of each cell; these plots correspond to the experimental results of Fig. 6.

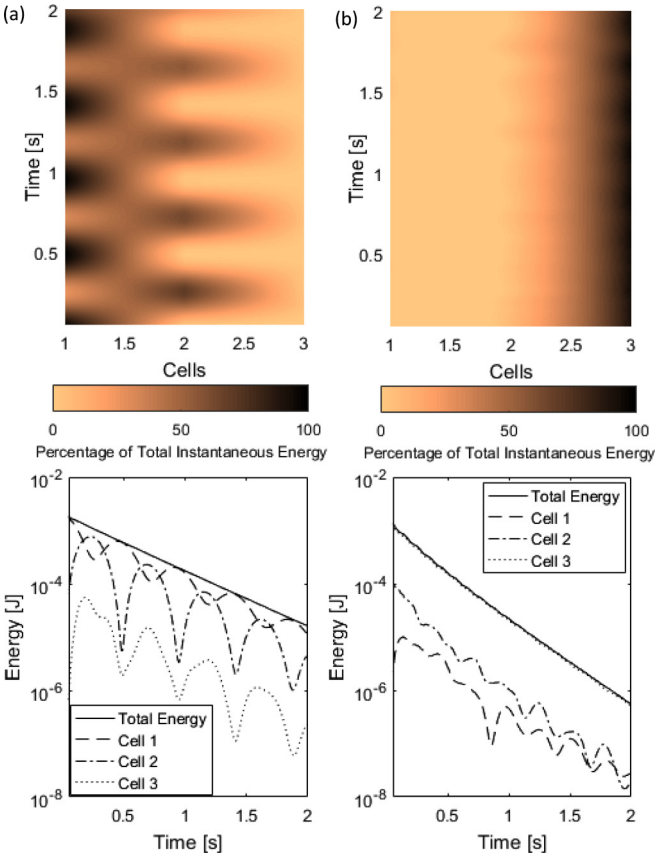

FIG. 11. Numerical simulation results of the ROM for intermediate impulsive intensity, impulsive magnitude 102.04 N applied to cell 1, and impulsive magnitude 96.19 N applied to cell 3: (a) spatiotemporal variation of normalized energy (with respect to input energy) for each cell, and (b) and temporal variations of the lattice energy and the non-normalized energy of each cell; these plots correspond to the experimental results of Fig. 7.

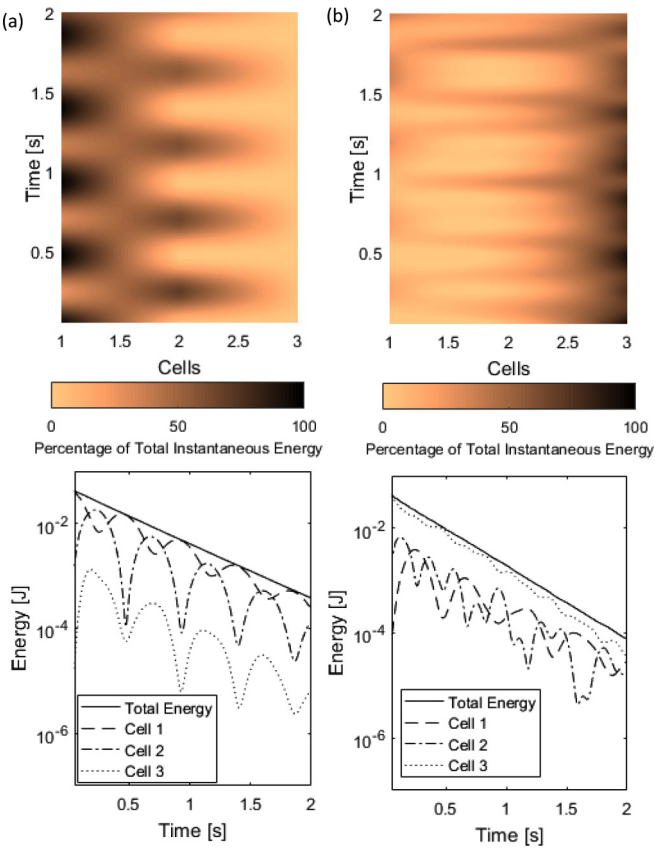

FIG. 12. Numerical simulation results of the ROM for large impulsive intensity, impulsive magnitude 856.99 N applied to cell 1, and impulsive magnitude 835.72 N applied to cell 3: (a) spatiotemporal variation of normalized energy (with respect to input energy) for each cell, and (b) and temporal variations of the lattice energy and the non-normalized energy of each cell; these plots correspond to the experimental results of Fig. 8.

maximum value of δ occurs experimentally at an impulse intensity of $\sim$250 N.

Third, we note good agreement between the experimental and computational nonreciprocity measures, with the exception of very large force intensities. In similarity to the experimental results, for the reduced-order model the corresponding measure of nonreciprocity δ is calculated using as measurement points the LSs of each cell. The experimental and simulated trends are in good agreement for low-to-intermediate impulse excitations but diverge for very large impulse excitations for measurement points involving cell 3. In addition, in contrast to the experimental results, no global maximum is predicted by the ROM simulation. Nonetheless, the satisfactory agreement between experiment and ROM simulations provides a first confirmation of the efficacy of the ROM to accurately predict and model the nonlinear nonreciprocal acoustics of the lattice up to intermediate impulse intensities.

As a final task of our study we study in detail the six-DOF mathematical ROM of the three-cell lattice discussed in Sec. II (with system parameters listed in Table I), with the aim to show that it accurately reproduces the experimental results. This provides confidence in the interpretation of the experimental results, but also validates the ROM as an accurate and reliable tool for predictive design of the lattice, e.g., for optimization of global acoustic nonreciprocity according to certain criteria.

In Fig. 10 we depict the results of the numerical simulations of the ROM for the case of low-intensity impulsive excitation corresponding to the results of Fig. 6. To perform these simulations we considered two separate impulsive excitations, first applied to unit cell 1 and then to unit cell 3, respectively. Moreover, the actual experimentally measured impulsive leads corresponding to the plots of Fig. 6 were used in each of these simulations, in order to get a direct comparison between simulation and experiment. These results agree with the corresponding experimental results of Fig. 6 both qualitatively and quantitatively. The ROM accurately predicts L-R wave propagation and response localization depending on the point of application of the excitation. In addition, the nonlinear energy exchanges or beats between cells during L-R wave propagation [cf. the left plot of Fig. 10(b)] are accurately reproduced by the ROM.

Similar conclusions are drawn from the ROM results depicted in Figs. 11 and 12, corresponding to the experimental results of Figs. 7 and 8, respectively. For intermediate impulsive excitation (cf. Fig. 11) the ROM simulations confirm L-R wave propagation for cell 1 excitation and response localization

for cell 3 excitation. For strong impulsive excitation (cf. Fig. 12), the ROM accurately predicts both L-R and R-L wave propagation, in accordance to the experiments (cf. Fig. 8); also the energy exchanges between cells are recovered. The ROM simulation, however, predicts that a portion of the impulse energy remains localized while the same is not observed in the experiment. This might explain the divergence between computation and experiment of the nonreciprocity measure δ for high impulse intensities that is observed in the plots of Fig. 9.

V. CONCLUDING REMARKS

Following the theoretical and experimental study of *local* dynamic nonreciprocity in a hierarchical nonlinear unit cell [20], and the theoretical study of *global* acoustic nonreciprocity in a lattice of coupled unit cells [23], in this work we presented the experimental validation of global acoustic nonreciprocity in a three-cell lattice with unit cells incorporating a large scale (LS) and a small scale (SS).

The experimental results confirmed the theoretical predictions: For sufficiently small-to-intermediate applied impulsive loads there occurred L-R wave propagation in the hierarchical lattice, but nonlinear localization prevented an analogous R-L wave propagation. For strong applied impulses, however, both L-R and R-L wave propagation occurred in the lattice, although strong nonreciprocity still persisted in the lattice. A reduced-order model (ROM) derived from system identification and characterization of the unit cells accurately reproduced the experimental findings, and was validated as a useful computational tool for parametrically studying and optimizing global acoustic nonreciprocity in the lattice.

Such an optimization study is closely tied to building an understanding of the nonlinear mechanism that gives rise and governs global acoustic nonreciprocity in the nonlinear, asymmetric, and hierarchical lattice. As proven in [20] the nonlinear mechanism governing local nonreciprocity in each unit cell is 1:1 resonance capture between the LS and SS dynamics. Accordingly, it is logical to assume that a similar resonance capture mechanism would be responsible for the global acoustic nonreciprocity in the lattice. This conjecture agrees with the numerical observation that wave propagation in the lattice is in the form of traveling breathers possessing a dominant "fast" frequency. In addition, the generation of nonlinear localization in the rightmost unit cell for sufficiently small impulsive loads needs to be examined, together with the bifurcations that cause its elimination as the applied impulse increases and R-L wave propagation commences in the lattice. Such a study can be performed by asymptotic analysis of the acoustics of the derived ROM. Moreover, the effect on acoustic nonreciprocity of the adding of more internal scales (i.e., more SSs of increasingly smaller mass—cf. Fig. 1) in the hierarchical structure of each unit cell needs to be studied.

In synopsis, the presented experimental results validate the existence of nonlinear acoustic nonreciprocity in the proposed lattice. As such, they promote an alternative passive paradigm for realizing acoustic nonreciprocity in a broad class of nonlinear hierarchical lattice systems, without requiring external sources of energy (e.g., external biases or time-varying system properties) as current applications do. However, the role and interplay of internal hierarchy, asymmetry, and nonlinearity in such nonreciprocity need to be more closely investigated.

ACKNOWLEDGMENTS

This work was funded in part by the National Science Foundation Emerging Frontiers Research Initiative (EFRI) Grant No. 1741565. K.J.M. is grateful for the support of the National Science Foundation Graduate Research Fellowship under Grant No. DGE-1144245.

Any opinion, findings, and conclusions or recommendations expressed in this material are those of the authors(s) and do not necessarily reflect the views of the National Science Foundation.

[1] H. von Helmholtz, *Theorie der Luftschwingungen in Röhren mit offenen Enden* (W. Engelmann, Leipzig, 1896), p. 80.
[2] J. Strutt, Proc. London Math. Soc. **1**, 357 (1871).
[3] R. Courant and D. Hilbert, *Methods of Mathematical Physics* (Interscience, New York, 1965), Vol. 1; original title: *Methoden der mathematischen Physik*.
[4] H. B. G. Casimir, Rev. Mod. Phys. **17**, 343 (1945).
[5] L. Onsager, Phys. Rev. **37**, 405 (1931).
[6] L. Onsager, Phys. Rev. **38**, 2265 (1931).
[7] R. Fleury, D. Sounas, M. R. Haberman, and A. Alù, Acoustics Today **11**, 14 (2015).
[8] R. Fleury, D. L. Sounas, C. F. Sieck, M. R. Haberman, and A. Alù, Science **343**, 516 (2014).
[9] S. A. Cummer, Science **343**, 495 (2014).
[10] K. Tsakmakidis, L. Shen, S. Schulz, X. Zheng, J. Upham, X. Deng, H. Altug, A. Vakakis, and R. Boyd, Science **356**, 1260 (2017).
[11] B.-I. Popa and S. A. Cummer, Nat. Commun. **5**, 3398 (2014).
[12] R. Fleury, D. L. Sounas, and A. Alù, Phys. Rev. B **91**, 174306 (2015).
[13] B. Liang, X. Guo, J. Tu, D. Zhang, and J. Cheng, Nat. Mater. **9**, 989 (2010).
[14] N. Boechler, G. Theocharis, and C. Daraio, Nat. Mater. **10**, 665 (2011).
[15] M. Maldovan, Nature **503**, 209 (2013).
[16] F. Li, P. Anzel, J. Yang, P. G. Kevrekidis, and C. Daraio, Nat. Commun. **5**, 5311 (2014).
[17] J. Zhang, B. Peng, Ş. K. Özdemir, Y.-X. Liu, H. Jing, X.-Y. Lü, Y.-L. Liu, L. Yang, and F. Nori, Phys. Rev. B **92**, 115407 (2015).
[18] A. Blanchard, T. P. Sapsis, and A. F. Vakakis, J. Sound Vib. **412**, 326 (2018).
[19] Z. Zhang, I. Koroleva, L. I. Manevitch, L. A. Bergman, and A. F. Vakakis, Phys. Rev. E **94**, 032214 (2016).
[20] K. J. Moore, J. Bunyan, S. Tawfick, O. V. Gendelman, S. Li, M. Leamy, and A. F. Vakakis, Phys. Rev. E **97**, 012219 (2018).
[21] G. B. Whitham, *Linear and Nonlinear Waves* (John Wiley & Sons, New York, 2011), Vol. 42.
[22] L. I. Manevitch and A. F. Vakakis, SIAM J. Appl. Math. **74**, 1742 (2014).

[23] M. D. Fronk, S. Tawfick, C. Daraio, A. F. Vakakis, and M. J. Leamy, in *ASME 2017 International Design Engineering Technical Conferences and Computers and Information in Engineering Conference, Vol. 8* (American Society of Mechanical Engineers, New York, 2017), p. V008T12A023.
[24] J. P Mücket, Astron. Nachr. **310**, 379 (1989).
[25] A. F. Vakakis and O. Gendelman, J. Appl. Mech. **68**, 42 (2001).
[26] A. F. Vakakis, O. V. Gendelman, L. A. Bergman, D. M. McFarland, G. Kerschen, and Y. S. Lee, *Nonlinear Targeted Energy Transfer in Mechanical and Structural Systems*, Solid Mechanics and Its Applications Vol. 156 (Springer Science & Business Media, Dordrecht, 2008).
[27] D. M. McFarland, L. A. Bergman, and A. F. Vakakis, Int. J. Non-Linear Mech. **40**, 891 (2005).
[28] H. Cho, M.-F. Yu, A. F. Vakakis, L. A. Bergman, and D. M. McFarland, Nano Lett. **10**, 1793 (2010).
[29] S. Masri and T. Caughey, J. Appl. Mech. **46**, 433 (1979).
[30] G. Kerschen, V. Lenaerts, and J.-C. Golinval, Mech. Syst. Signal Process. **17**, 189 (2003).
[31] G. Kerschen, K. Worden, A. F. Vakakis, and J.-C. Golinval, Mech. Syst. Signal Process. **20**, 505 (2006).
[32] J.-P. Noël and G. Kerschen, Mech. Syst. Signal Process. **83**, 2 (2017).
[33] S. A. Hubbard, D. M. McFarland, L. A. Bergman, A. F. Vakakis, and G. Andersen, AIAA J. **52**, 2633 (2014).
[34] C. A. Herrera, D. M. McFarland, L. A. Bergman, and A. F. Vakakis, J. Sound Vib. **388**, 298 (2017).